Investigating the potential of drift tube ion mobility for the analysis of oxidized lipids

Investigating the potential of drift tube ion mobility for the analysis of oxidized lipids

Katyeny Manuela da Silva[1*], Michele Wölk[2], Palina Nepachalovich[2], Elias Iturrospe[1,3], Adrian Covaci[1], Alexander L.N. van Nuijs[1*], Maria Fedorova[2*]

[1]Toxicological Centre, University of Antwerp, Universiteitsplein 1, 2610 Antwerp, Belgium

[2] Lipid Metabolism: Analysis and Integration, Center of Membrane Biochemistry and Lipid Research, Faculty of Medicine Carl Gustav Carus of TU Dresden, 01307, Dresden, Germany

[3] Department of In Vitro Toxicology and Dermato-cosmetology, Vrije Universiteit Brussel, Laarbeeklaan 103, 1090, Jette, Belgium

*Corresponding authors: manuellam31@gmail.com, alexander.vannuijs@uantwerpen.be, maria.fedorova@tu-dresden.de

Abstract

Epilipids, a subset of the lipidome that comprises oxidized, nitrated, and halogenated lipid species, show important biochemical activity in the regulation of redox lipid metabolism by influencing cell fate decisions including death, health, and aging. Due to the large chemical diversity, reversed-phase liquid chromatography-high resolution mass spectrometry (RPLC-HRMS) methods have only a limited ability to separate numerous isobaric and isomeric epilipids. Ion mobility spectrometry (IMS) is a gas-phase separation technique that can be combined with LC-HRMS to improve overall peak capacity of the analytical platform. Here, we illustrate the advantages and discuss the current limitations of implementing IMS in LC-HRMS workflows for the analysis of oxylipins and oxidized complex lipids. Using isomeric mixtures of oxylipins we demonstrated that while deprotonated ions of eicosanoids poorly resolved by IMS, sodium acetate and metal adducts (e.g., Li, Na, Ag, Ba, K) of structural isomers often showed ΔCCS% above 1.4% and base peak separation with high resolution demultiplexing (HRDm). The knowledge of the IM migration order was also used as proof of concept to help in the annotation of oxidized complex lipids using HRDm and All Ions Fragmentation spectra. Additionally, we utilized a mixture of deuterium-labeled lipids for a routine system suitability test with the purpose of improving harmonization and interoperability of IMS datasets in (epi)lipidomics.

Keywords: oxylipins, lipids, collision cross section, ion mobility spectrometry, oxidized lipids

1. Introduction

The role of lipid modifications in the regulation of the metabolism, cell fitness, health, and senescence has aroused interest in epilipids, a subset of the lipidome that includes oxidized, nitrated, and halogenated lipids produced via enzymatic and non-enzymatic reactions.[1] Among them, oxylipins are a structurally diverse class of bioactive oxygenated fatty acid metabolites that can be found in free or esterified forms. Unlike their non-enzymatically produced analogs (e.g., isoprostanes), oxylipins are products of enzyme-mediated reactions with defined stereospecificity and chirality for each functional group.[2] Thus, the large chemical diversity of free and esterified oxylipins including multiple isomeric species, poses major analytical challenges. Typically, targeted mass spectrometry (MS) methods based on multiple reaction monitoring (MRM) are used for the detection and quantification of oxylipins for which analytical standards are available.[3] Besides the good sensitivity and selectivity of targeted methods, untargeted methods are very valuable for the discovery of new free and esterified oxylipins and their potential biological functions.[4] In this context, high-resolution tandem MS (HRMS) is usually the method of choice for species-level identification of lipids in an untargeted manner. [5,6] A data-dependent acquisition (DDA) strategy can be applied to obtain tandem mass spectra used to define the lipid class, fatty acyl composition, and even to deeper characterize epilipids including the type (e.g., epoxy- (ep), keto- (oxo), hydroxy- (OH)) and the position of modification in complex modified glycerophospholipids (GPL), glycerolipids (GL), and cholesteryl esters (CE). [7,8]

However, efficient separation of isomeric and isobaric species prior to MS/MS acquisition is crucial to obtain tandem mass spectra suitable for such accurate annotation. Commonly used ultra-high-performance chromatography provides high separation efficiency combined with a short analysis time. However, with such a high-throughput approach many isomeric and isobaric species remain unresolved.[9,10] More specialized separation options were developed for oxylipin analysis. For instance, chiral chromatography on a polysaccharide-based column compatible with reversed-phase liquid chromatography (RPLC) solvents was applied to separate eicosanoid enantiomers.[11,12] More recently, chiral supercritical fluid chromatography-tandem mass spectrometry (SFC-MS/MS) was used to separate complex stereoisomer mixtures of octadecanoids.[13] Furthermore, orthogonal separations based on two-dimensional chromatography (2D-LC) were evaluated for the analysis of complex mixtures.[14] The combination of an amylose-based tris(3,5-dimethylphenylcarbamate) chiral column in the first dimension and a C18 RP column in the second dimension provided comprehensive orthogonal LC×LC analysis of oxylipins, however at the cost of long analysis time (3 h per sample) and low sensitivity due to dilution effects.[15]

Ion mobility spectrometry (IMS), a gas-phase technique separating ionized analytes based on a size, shape, and charge, has shown promising results in the separation of isobaric and isomeric lipids (e.g., *sn*-positions, cis/trans orientations, and R/S positions).[16] In addition to increasing the overall peak capacity of the analytical platform by coupling IMS to LC-HRMS, collision cross section (CCS) values can be derived

from the measured mobility and used to support untargeted annotation workflows.[17,18] Ion mobility experiments can be performed using time-dispersive, spatial-dispersive, or confinement-selective release instrumentation.[19] While the time-dispersive instruments with static (e.g., drift tube (DTIMS)) or oscillating electric field (e.g., traveling wave (TWIMS)) have been widely used in lipidomics,[20] new instruments have been introduced mainly to improve the resolution of IMS separation (e.g., cyclic IMS).[21,22] Alternatively, a post-acquisition strategy known as high resolution demultiplexing (HRDm) has been shown to increase the DTIMS platform's resolving power through the interpolation of time-of-flight (TOF) transients and demultiplexing algorithms.[23]

With epilipid standards being scarce, structural elucidation often relies solely on RPLC behavior and MS/MS fragmentation patterns.[1] Thus, the availability of CCS values could further increase the level of confidence in epilipid annotations. In this study, the IM behavior of several isomeric groups of eicosanoids (Figure 1) was evaluated using DTIMS separation. Although oxylipins are traditionally analyzed in negative ionization mode[24], we additionally explored analysis in positive ionization mode by introducing various metal adducts. These modifications can alter the 3D gas-phase structure of the ions and thus may influence the MS/MS fragmentation mechanisms and the ion mobility separation.[25,26]

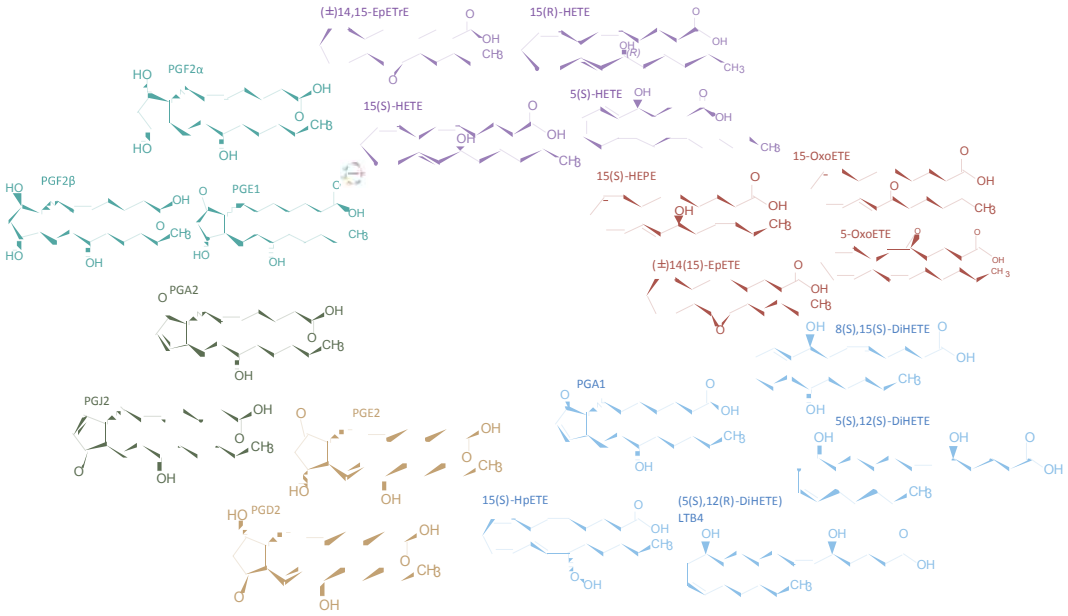

Figure 1. Examples of oxidized metabolites of arachidonic acid (FA 20:4). 5(S)-HETE: 5S-hydroxyeicosatetraenoic acid. 15(R)-HETE: 15R-hydroxy-5Z,8Z,11Z,13E-eicosatetraenoic acid. 15(S)-HETE: 15S-hydroxy-5Z,8Z,11Z,13E-eicosatetraenoic acid. 14,15-EpETrE: 14,15-epoxy-5Z,8Z,11Z-eicosatrienoic acid. 5-OxoETE: 5-oxo-6E,8Z,11Z,14Z-eicosatetraenoic acid. 14(15)-EpETE: (+/-)-14(15)-epoxy-5Z,8Z,11Z,17Z-eicosatetraenoic acid. 15-OxoETE: 15-oxo-5Z,8Z,11Z,13E-eicosatetraenoic acid. 15(S)-HEPE: 15S-hydroxy-5Z,8Z,11Z,13E,17Z-eicosapentaenoic acid. PGE2: 9-oxo-11R,15S-dihydroxy-5Z,13E-prostadienoic acid. PGD2: 9S,15S-dihydroxy-11-oxo-5Z,13E-prostadienoic acid. PGJ2: 11-oxo-15S-hydroxy-5Z,9,13E-prostatrienoic acid. PGA2: 9-oxo-15S-hydroxy-5Z,10Z,13E-prostatrienoic acid. PGE1: 9-oxo-11R,15S-dihydroxy-13E-prostaenoic acid. PGF2α: 9S,11R,15S-trihydroxy-5Z,13E-prostadienoic acid. PGF2β: 9R,11R,15S-trihydroxy-5Z,13E-prostadienoic acid. 15(S)-HpETE: 15S-hydroperoxy-5Z,8Z,11Z,13E-eicosatetraenoic acid. PGA1: 9-oxo-15S-hydroxy-10Z,13E-prostadienoic acid. 5(S),12(S)-DiHETE: 5S,12S-dihydroxy-6E,8Z,10E,14Z-eicosatetraenoic acid. 8(S),15(S)-

DiHETE: 8S,15S-dihydroxy-5Z,9E,11Z,13E-eicosatetraenoic acid. 5(S),12(R)-DiHETE (LTB4): 5S,12R-dihydroxy-6Z,8E,10E,14Z-eicosatetraenoic acid.

2. Materials And Methods

2.1. Chemicals

Methanol ultrapure (MeOH), acetonitrile (MeCN), isopropanol (i-PrOH), and formic acid (99%, HCOOH), all UPLC/MS grade were purchased from Biosolve (Valkenswaard, the Netherlands). Ammonium acetate (CH_3COONH_4), ammonium formate ($HCOONH_4$), acetic acid (CH_3COOH), and ethanol (EtOH), all LC-MS grade, copper(II) sulfate pentahydrate ($CuSO_4 \cdot 5H_2O$), ammonium bicarbonate (NH_4HCO_3) potassium acetate (CH_3COOK), sodium acetate (CH_3COONa), barium acetate ($(CH_3COO)_2Ba$), silver acetate (CH_3COOAg), lithium acetate (CH_3COOLi) and chloroform ($CHCl_3$, analytical grade) were obtained from Sigma-Aldrich (Darmstadt, Germany). Ultrapure water (H_2O) used throughout the experiments was obtained from an Elga Pure Lab apparatus (Tienen, Belgium).

Oxylipins (Table 1 and Supporting Information (SI)-1.1) were purchased from Cayman Chemical (Ann Arbor, Michigan, United States). 1-palmitoyl-2-linoleoyl-*sn*-glycero-3-phosphocholine (PC 16:0/18:2), 1-palmitoyl-2-oleoyl-*sn*-glycero-3-phosphocholine (PC 16:0/18:1) and SPLASH® LIPIDOMIX® were purchased from Avanti Polar Lipids (Alabaster, United States). 1,2-dipalmitate-3-linoleate-glycerol (TG 16:0/16:0/18:2) and cholesteryl linoleate (CE 18:2) were acquired from Larodan (Solna, Sweden).

Table 1. Elemental compositions, mass and notations for 20 oxylipins used in the study.

Elemental composition (neutral)	Neutral Mass (Da)	Compound Abbreviation*	Notation (species level)
$C_{20}H_{34}O_5$	354.2406	PGE1	FA 20:3;O3
		PGF2α	
		PGF2β	
$C_{20}H_{32}O_3$	320.2351	14,15-EpETrE	FA 20:4;O
		15(R)-HETE	
		15(S)-HETE	
		5(S)-HETE	
$C_{20}H_{32}O_4$	336.2301	15(S)-HpETE	FA 20:4;O2
		5(S),12(S)-DiHETE	
		5(S),12(R)-DiHETE	
		8(S),15(S)-DiHETE	
		PGA1	
$C_{20}H_{32}O_5$	352.2250	PGD2	FA 20:4;O3
		PGE2	
$C_{20}H_{30}O_3$	318.2195	14(15)-EpETE	FA 20:5;O
		15(S)-HEPE	
		15-OxoETE	
		5-OxoETE	
$C_{20}H_{30}O_4$	334.2144	PGA2	FA 20:5;O2
		PGJ2	

*Abbreviations as described in Figure 1.

2.2. Data Acquisition

Analytical measurements were performed on an Agilent 1290 Infinity II LC system coupled to an Agilent 6560 drift tube ion mobility (DTIM)-quadrupole-time of flight (QTOF)-MS with dual jet stream electrospray ionization (ESI) source. Experiments were performed with flow injection analysis (FIA) or chromatographic separation with a Thermo Scientific Accucore C18 column (150 × 2.1 mm, 2.6 µm, 150 Å). Mobile phases (MP) consisted of MeCN/H_2O (1/1, v/v; A) and i-PrOH/MeCN/H_2O (85/10/5, v/v/v; B) supplemented either with 5 mM $HCOONH_4$ (MPF for formate supplemented MP) or 5 mM CH_3COONH_4 (MPAc for acetate supplemented MP) and 0.1% (v/v) HCOOH. The methods are described in detail in Table SI-2.1.

Ion mobility data were acquired using pseudorandom 4-bit multiplexing mode and data-independent acquisition (DIA) based on All Ions Fragmentation (AIF) alternating between no collision energy and high collision energy frames (AF) in the single pulse mode at 10, 20, and 40 eV. A calibrant solution (purine and hexakis(1H, 1H, 3H-tetrafluoropropoxy)phosphazine) was constantly infused with an isocratic pump (Agilent 1260 Infinity II Isocratic Pump (G7110B)). The Agilent tune mixture (G1969-85000) was infused at regular intervals to obtain the slope and intercept of the calibration function used to calculate the $^{DT}CCS_{N2}$ values of (un)known compounds acquired with the same electric field. All measurements were performed in triplicate.

2.3. Preparation of oxylipin solutions and in vitro oxidation of lipids

Oxylipin standards (Table 1) were dissolved to obtain a concentration of 1 µg/mL, followed by a serial dilution of 1:10, 1:100, and 1:1000. For the analysis in negative ion mode, oxylipin standard solutions were diluted in 10% B using either MPF or MPAc solvent systems to generated formate or acetate adducts upon ESI, respectively. The solutions of Li, Ba, Na, K, or Ag acetate salts were first prepared in ultrapure H_2O (10 mM), then diluted to 1 mM with MPF-A/MPF-B (9/1, v/v) to dissolve and generate cationized oxylipins. For *in vitro* oxidation of complex lipids, the protocol was adapted from the previous work by Criscuolo *et al*.[8] Briefly, lipids for preparation of micelles (0.5 mg of TG 16:0/16:0/18:2 with 0.15 mg of PC 16:0/18:1, or 0.5 mg of CE 18:2 with 0.19 mg of PC 16:0/18:1) and liposomes (0.5 mg of PC 16:0/18:2 or PC 16:0/20:4) were dried under a stream of N_2. A total of 500 µL of 3 mM NH_4HCO_3 (pH 7.5) was added, vortexed for 10 s, and sonicated for 15 min. Next, 250 µL of 1.2 mM $CuSO_4 \cdot 5H_2O$ and 250 µL of 2.4 mM Na-L-ascorbate were added to each sample. Samples were incubated for 24 h using an Eppendorf Thermo Mixer (37°C, 450 rpm). Aliquots (250 µL) were collected and 500 µL of MeOH/$CHCl_3$ (1/1, v/v) was added for extraction, vortexed, and centrifuged for 10 min at 4000 g at room temperature. The lower phase was collected, dried under N_2, and dissolved in 250 µL of i-PrOH/H_2O (90/10, v/v) and further diluted to 1:10 and 1:100.

2.4. Data Processing

All data were post-processed for calibration of the mass axis using purine (*m/z* 121.0508 in ESI(+) mode and *m/z* 119.0363 in ESI(−) mode) and hexakis(1H, 1H, 3H-tetrafluoropropoxy)phosphazine (*m/z* 922.0097 in ESI(+) mode and *m/z* 980.0163 in ESI(−) mode) in IM-MS Reprocessor software (Agilent Technologies, Santa Clara, U.S.A). Next, data files were processed with PNNL PreProcessor[27], and single-field collision cross-section values were calculated using IM-MS Browser v.10.00 (Agilent). To enhance the resolving power of DTIM measurements, high resolution demultiplexing 2.0 (Agilent) was used after the data was demultiplexed (PNNL PreProcessor with data interpolation of 1 to 3 drift bins) and a feature list was generated for each demultiplexed file in IM-MS Browser v.10.00.[28] In order to identify data artifacts that can be generated during post-processing with HRDm, the compounds were injected individually and in mixtures at different concentrations. The isotopic pattern of compounds was manually confirmed, and the individual standards were plotted over the IM resolved peaks of mixtures. The percent difference in CCS (ΔCCS%) was used to evaluate the degree of separation for isomeric pairs at a given single peak resolving power.[28,29]

3. Results and Discussion

3.1. Quality control for IMS experiments

Quality control (QC) procedures are essential to ensure data robustness in untargeted analysis. Although CCS values can be considered a physiochemical property of an ion in the gas phase, experimental values can vary up to 6.2% depending on the technique used for data acquisition.[30] In addition, more than one peak can be observed in the IM for the compound of interest due to multiple ionization sites or simply because of the presence of poorly resolved isobaric ions or co-eluting isomers. As a result, peak selection and annotation for database building for IM should be performed with a manual (visual) inspection of the IM spectra using a minimum of three replicates to assess the repeatability. Guidelines are available for peak annotation and reporting (e.g., gas and electric field used, calibration strategy, and composition of the calibration solution) in IM.[31–33] The latter also includes the use of a system suitability sample to generate reference values and assess systematic deviations during data acquisition and interlaboratory studies.[32] However, the current CCS compendium's compound list for quality assessment relies on small polar molecules like amino acids and peptides, with only a single lipid (cortisol) represented (https://mcleanresearchgroup.shinyapps.io/CCS-Compendium/). As such, the CCS Compendium is not an ideal reference for lipidomics IM analysis since instrumental conditions can be significantly different when analyzing lipids compared to polar small molecules.[34]

Here, the use of a deuterium-labeled mixture of lipid standards is introduced as a quality control/system suitability sample for IM.[35,36] Therefore, the components of the SPLASH® Lipidomix® Mass Spec Standard, including eight lipids for ESI(+) and five for ESI(−) mode, were considered for the evaluation (Table 2). Since two different mobile phases (MPF and MPAc) were used and some lipids tend to form adducts with acetate and/or formate in ESI(−), both types of adducts ($[M+CH_3COO]^-$ and $[M+HCOO]^-$) were included. In each batch, the mixture of reference labeled standards was injected three times, i.e., in the beginning, the middle, and at the end of each sequence. Interlaboratory studies using DTIMS reported relative standard deviation (RSD) values of 0.3%.[32] Therefore, the average $^{DT}CCS_{N2}$, SD, and RSD were calculated and an RSD $\leq$ 0.1% was chosen as an acceptable precision for intra-day measurements of standards (N=3). If the RSD value was exceeded, the standard was reinjected together with the tune mix for the calibration. In terms of accuracy, the average $^{DT}CCS_{N2}$ measurements were compared with available data in the CCS Compendium and the average percentage error was 0.5% with a maximum of 0.9% for all compounds (Table 2). As a result, the suitability criterium of CCS error < 1.0% was fulfilled.[31] Thus, the application of certified mixture of standards (here SPLASH® Lipidomix® Mass Spec Standard) as a routine system suitability measure helps to ensure the QC between and within IMS data acquisition within one laboratory. Reporting the CCS values of different lipid classes in IM databases (e.g., LIPID MAPS® Lipidomic Ion Mobility Database) can improve harmonization and interoperability of IMS datasets.

Table 2. Simplified system suitability mixture with the experimental average collision cross section (CCS) values and available reference values in the CCS Compendium. SD: Standard Deviation. RSD: Relative Standard Deviation **N*=3. NA: Not Available.

Compound	Formula	Ion Species	Theoretical *m/z*	Average CCS (Å²)*	SD (Å²)	RSD (%)	CCS compendium	Error (%)
CE 18:1(d7)	C45H71D7O2	[M+Na]+	680.6333	292.47	0.15	0.05	291.8	0.2
DG 15:0/18:1(d7)	C36H61D7O5	[M+Na]+	610.5398	256.97	0.06	0.02	259.0	0.8
LPC 18:1(d7)	C26H45D7NO7P	[M+CH_3COO]-	587.4059	246.40	0.10	0.04	NA	-
		[M+H]+	529.3994	232.70	0.10	0.04	234.9	0.9
		[M+HCOO]-	573.3903	242.17	0.15	0.06	NA	-
LPE 18:1(d7)	C23H39D7NO7P	[M+H]+	487.3524	216.37	0.06	0.03	217.8	0.7
PC 15:0/18:1(d7)	C41H73D7NO8P	[M+CH_3COO]-	811.6199	291.70	0.00	0.00	292.6	0.3
		[M+HCOO]-	797.6043	288.83	0.06	0.02	289.6	0.3
		[M+H]+	753.6134	285.17	0.21	0.07	285.4	0.1
PE 15:0/18:1(d7)	C38H67D7NO8P	[M-H]-	709.5519	264.47	0.15	0.06	266.9	0.9
		[M+H]+	711.5664	271.70	0.17	0.06	273.5	0.7
PG 15:0/18:1(d7)	C39H68D7O10P	[M-H]-	740.5464	271.03	0.06	0.02	NA	-
PI 15:0/18:1(d7)	C42H72D7O13P	[M-H]-	828.5625	285.60	0.10	0.04	NA	-
SM 18:1;2O/18:1(d9)	C41H72D9N2O6P	[M+CH_3COO]-	796.6536	292.37	0.06	0.02	NA	-
		[M+H]+	738.6470	287.47	0.06	0.02	NA	-
		[M+HCOO]-	782.6379	289.63	0.25	0.09	NA	-
TG 15:0/18:1(d7)/15:0	C51H89D7O6	[M+NH_4]+	829.7985	311.97	0.15	0.05	NA	-

3.2. Ion mobility behavior of isomeric oxylipins

To be efficiently resolved by IM, isomeric compounds must have significantly different conformations in the cross-section space that can be differentiated with a given instrumental resolution. Enantiomers typically require higher resolving power for base peak separation, followed by cis/trans (*Z/E*) and constitutional isomers.[29] However, the efficiency of isomer separation based on IM is highly dependent on the structure of the molecule.[37] For instance, *Z/E* isomers of diacylglycerophospholipids show better IM separation than the constitutional isomeric pesticides terbuthylazine and propazine.[38] Therefore, the IM behavior for the analytes of interest should be assessed experimentally to evaluate what type of isomeric separation by IM can be achieved.

Here we explore the CCS space for 20 eicosanoids corresponding to six groups of isomers in negative and positive ionization modes (Table 1, Figure 1). Oxylipins ionize well in the ESI(-) mode as deprotonated species as well as deprotonated CH_3COONa adducts when ammonium acetate is supplemented in the mobile phase.[4] In ESI(+) mode, some oxylipins can form protonated species or metal adducts.[39] Metal adducts can alter the gas-phase conformation of molecules, offering the potential for the separation of isomers, such as bile acids and cannabinoids.[40,41] Thus, we investigated the effect of Li, Na, K, Ag, and Ba adducts on oxylipins IM separation. The list of experimental $^{DT}CCS_{N2}$ values for 134 measured different ionization species is provided in Table SI-1.

Previously reported CCS space for lipids typically range from 150 to 400 Å^2 [17,42], withing which oxylipins, in our study, occupied the range between 178.60 to 208.03 Å^2. The ΔCCS% of each isomeric pair was calculated to assess the ionization mode (positive/negative) and ionization species with the highest separation efficiency (Table SI-1.2). Both $[M-H]^-$ and $[M+H]^+$ ions showed poor IM separation within isomeric groups. The only pairs of protonated ions with ΔCCS% > 2% were 5-OxoETE vs 15-OxoETE (ΔCCS% = 2.73%; positional isomers), and 5-OxoETE vs 14,15-EpETE (ΔCCS% = 3.25%; functional group isomer). However, for the majority of the oxylipins, protonated species were not even observed. The $[M-H]^-$ isomeric species with the largest difference in the cross section space were prostaglandins A2 and J2 (ΔCCS% = 1.91%; positional isomers). Interestingly, for the metal cations of oxylipins, 54 out of 56 isomeric pairs provided ΔCCS% > 2.0%, confirming that these ionization species are interesting candidates to explore IM separation.

3.2.1. IM separation of aliphatic acyclic oxidized fatty acids

Deprotonated ions of aliphatic acyclic metabolites, such as FA 20:4;O or FA 20:5;O isomeric groups, form very labile structures in the gas phase. Consequently, $[M-H]^-$ ions displayed broad IM peaks (e.g., 1-2 ms), and isomer separation was mostly not achieved. Thus, the deprotonated forms of aliphatic acyclic oxidized

fatty acids did not provide significant differences in CCS values, reflected in the similar arrival time distribution (ATD) of the individual standards (Figure 2 A-B).

However, a distinct IM behavior was observed for other ionization species. Acetate adducts $[M+CH_3COO]^-$ are commonly observed in ESI(−) mode for different lipid classes such as GPL, ceramides, and sphingomyelins when ammonium acetate is added to the mobile phase.[43] Using MPAc as mobile phase, the compounds in FA 20:4;O or FA 20:5;O isomeric groups formed $[M-H+CH_3COONa]^-$ ions at *m/z* 401.2304 and *m/z* 399.2148, respectively. The MS/MS spectra of $[M-H+CH_3COONa]^-$ adducts were acquired to confirm species identities (Figures SI-2.1 and SI-2.2). Similarly to the fragmentation pattern of $[M-H]^-$ ions, the typical neutral losses of H_2O and CO_2 and position-specific fragments were prominent in the MS/MS spectra of sodium acetate adducts upon collision-induced dissociation (CID).[8,44]

Importantly, sodium acetate adducts of constitutional isomers within FA 20:4;O and FA 20:5;O isomeric groups showed ΔCCS% above 1.4%. By comparing CCS values of sodium acetate anions for 14,15-EpETE vs 15(S)-HEPE, 15(S)-HETE, and 5(S)-HETE isomers, the ΔCCS% of 1.4, 1.6 and 2.4 % can be observed, respectively (Figure 2 C-D). Notably, the epoxy-modified lipids formed the most compact structure (as evidenced by shorter migration time/CCS) for both FA 20:4;O and FA 20:5;O sodium acetate adducts.

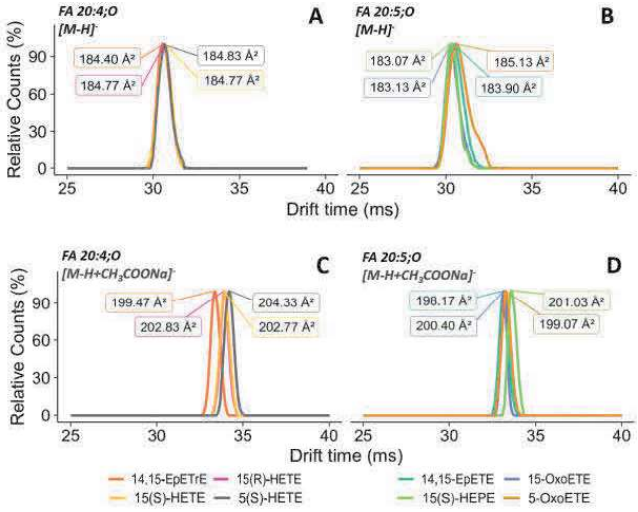

Figure 2. The arrival time distribution of the $[M-H]^-$ and $[M-H+CH_3COONa]^-$ ions of aliphatic acyclic oxidized fatty acid standards. 5(S)-HETE: 5S-hydroxyeicosatetraenoic acid. 15(R)-HETE: 15R-hydroxy-5Z,8Z,11Z,13E-eicosatetraenoic acid. 15(S)-HETE: 15S-hydroxy-5Z,8Z,11Z,13E-eicosatetraenoic acid. 14,15-EpETrE: 14,15-epoxy-5Z,8Z,11Z-eicosatrienoic acid. 5-OxoETE: 5-oxo-6E,8Z,11Z,14Z-eicosatetraenoic acid. 14(15)-EpETE: (+/-)-14(15)-epoxy-5Z,8Z,11Z,17Z-eicosatetraenoic acid. 15-OxoETE: 15-oxo-5Z,8Z,11Z,13E-eicosatetraenoic acid. 15(S)-HEPE: 15S-hydroxy-5Z,8Z,11Z,13E,17Z-eicosapentaenoic acid.

Although many successful applications for IM separation of a single pair of isomers are available, examples of IM separation of complex mixtures of isomers with more than three compounds are very scarce.[16,23] Here, a post-processing data reconstruction strategy based on 4-bit demultiplexed (Dm) DTIM files[23] was used to resolve the mixtures of four isomers. When FA 20:4;O isomers were analyzed as a mixture, the ATD of $[M-H+CH_3COONa]^-$ ions in this isomeric group showed that a high IM resolution ($R_p \approx 180$) is needed to resolve

constitutional isomers of aliphatic acyclic oxylipins (Figure 3A, black trace). However, by applying a high resolution demultiplexed (HRDm) strategy, we could obtain almost base peak separation (90%) of epoxy and hydroxy lipids with the modification at similar carbon atom positions (C_{14}-C_{15} for EpETrE and C_{15} for 15(S)-HETE and 15(R)-HETE) (Figure 3A, dashed trace). The 15-HETE enantiomers could not be resolved using HRDm, as expected based on a ΔCCS% of 0.03%. Interestingly, the positional isomers 15- and 5-HETE with a ΔCCS% of ≈ 1% could be successfully resolved using the HRDm approach.

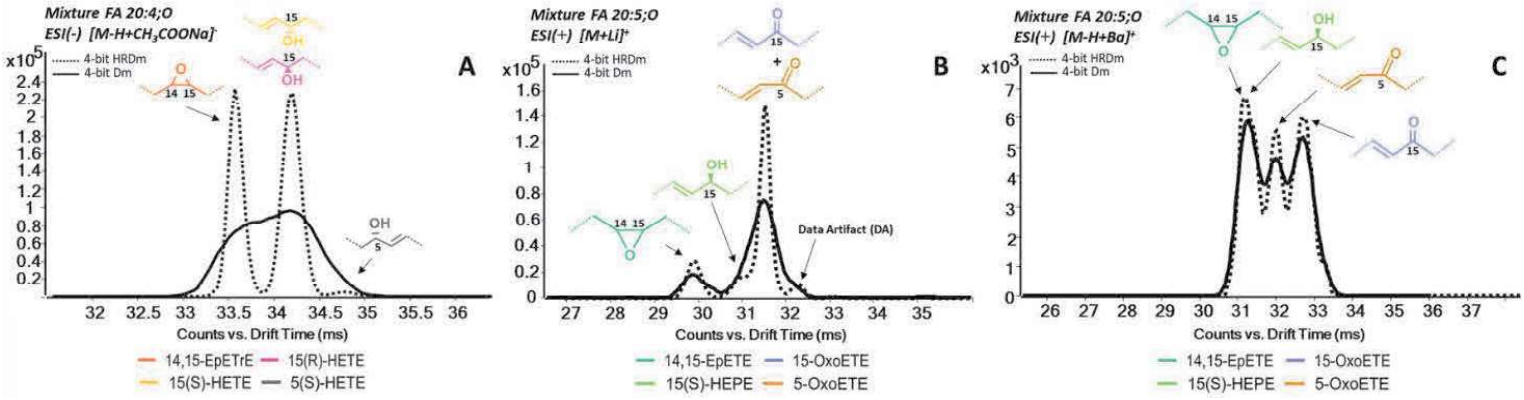

Figure 3. Arrival time distribution for the [M-H+CH_3COONa]$^-$ adducts of a mixture of isomeric oxidized fatty acid (FA) FA 20:4;O (A) and for the [M+Li]$^+$ and [M-H+Ba]$^+$ adducts of FA 20:5;O (B and C, respectively). The peaks were assigned based on the $^{DT}CCS_{N2}$ values. Dm: demultiplexing. HRDm: high resolution demultiplexing. 5(S)-HETE: 5S-hydroxyeicosatetraenoic acid. 15(R)-HETE: 15R-hydroxy-5Z,8Z,11Z,13E-eicosatetraenoic acid. 15(S)-HETE: 15S-hydroxy-5Z,8Z,11Z,13E-eicosatetraenoic acid. 14,15-EpETrE: 14,15-epoxy-5Z,8Z,11Z-eicosatrienoic acid. 5-OxoETE: 5-oxo-6E,8Z,11Z,14Z-eicosatetraenoic acid. 14(15)-EpETE: (+/-)-14(15)-epoxy-5Z,8Z,11Z,17Z-eicosatetraenoic acid. 15-OxoETE: 15-oxo-5Z,8Z,11Z,13E-eicosatetraenoic acid. 15(S)-HEPE: 15S-hydroxy-5Z,8Z,11Z,13E,17Z-eicosapentaenoic acid.

Compounds within the FA 20:5;O isomeric group appeared to have even more labile gas phase structures compared to FA 20:4;O, probably due to an additional double bond, negatively affecting the IM separation in ESI(−) even when HRDm strategy was applied. To improve the IM separation of this group, we explored the ionization in positive ion mode using metal ion adducts. As a result, a ΔCCS% > 2.0% was achieved for five out of six possible combinations of FA 20:5;O isomeric pairs using either [M+Li]$^+$ or [M-H+Ba]$^+$ species (Figure 3B-3C; SI-1.2). The MS/MS of [M-H+Ba]$^+$ and [M+Li]$^+$ adducts of FA compounds were acquired at different CID energies (5 to 40 eV) and representative spectra of individual standards are provided in Figures SI-2.3 to SI-2.5. However, they were not as informative as the spectra in negative mode. Interestingly, the intensity of [M-H+Ba]$^+$ was approximately one hundred times lower than the [M+Li]$^+$ mixture which can be explained by the compound's higher affinity for lithium or by the higher solvation of Ba^{2+} during ionization (Figure 3B-3C).[45] The differences in relative intensities and IM resolution of isomers for Li and Ba adducts suggest that the cationization might occur at different positions within the molecule. While Li can be coordinated via ion-dipole (epoxy) and ion dipole/π-interaction (hydroxy/keto modification

with alkene group vicinal to oxygen), Ba can form a cationized carboxylate which might induce different gas-phase conformations, and thus, promote the separation of particular isomers.[44]

The ATD and IM spectra of FA 20:5;O and FA 20:4,O mixtures showed that different ionization species can also affect the type of isomeric separation (Figures 3 and SI-2.6A). When the type of modification (ep, oxo, OH) occurring at the same carbon position (e.g., C_{14}-C_{15}, C_{15}) was investigated, the $^{DT}CCS_{N2}$ values of epoxy isomers were lower than hydroxy or keto in ESI(+). This indicates that the epoxy modification induces the most compact structures in the gas phase for protonated or metal-containing ions, which is also consistent with publicly available CCS values for oxylipins $[M+Na]^+$ (Table SI-1.3).[46] Meanwhile, keto modification formed the most open conformations with all detected adducts in ESI(+) based on their arrival time distribution. Although limited IM separation for $[M-H]^-$ did not provide clear trends, but keto-modified species showed a slightly more compact structure than hydroxy species also for the $[M-H+CH_3COONa]^-$ adducts (Figure 2D).

Despite the dataset's current size limitation, it demonstrateds the potential of using IM as an orthogonal method to RPLC in the analysis of oxidized lipids. Thus, the IM behavior appeared to be different from the RPLC elution order, in which the epoxy-modified lipids elute after hydroxy and keto derivatives (i.e., RPLC elution order: OH < oxo < ep).[8] The IM migration order of positional isomers varied for different ionization species. Hydroxy and keto isomers with modification located close to the ω-end of the acyl chain showed lower CCS values as $[M-H]^-$ (Table SI-1.3; literature values and Table SI-1.1).[46] This latter IM pattern, however, was not maintained for cationized compounds in ESI(+) or sodium acetate adducts in ESI(−). The mobility trends observed in this work are consistent with previous research involving the $[M+Na]^+$ adducts of oxylipins (5-HETE and 8-HETE < 12-HETE)[46] and HETE-esterified PC (IM migration order: PC 18:0/8-HETE and PC 18:0/9-HETE < PC 18:0/11-HETE and PC 18:0/12-HETE < PC 18:0/15-HETE)[4], but more data is required to predict accurate IM trends using machine learning.[47] This emphasizes the significance of high-quality CCS databases for oxidized lipids starting with oxylipins since they might induce similar migration patterns in complex epilipids.

3.2.2. IM separation of prostaglandins

Prostanoids are bioactive products of arachidonic acid metabolism synthesized by cyclooxygenases and prostaglandin synthases.[48] Prostaglandins, a subclass of prostanoids, have a distinctive cyclopentane ring between C_8 - C_{12} that influences their IM behavior. For example, the IM analysis of the FA 20:4;O2 isomeric group as $[M+Na]^+$ or $[M-H+2K]^+$ demonstrated that dihydroxy (2OH) and hydroperoxy (OOH) isomers have more compact structures than prostaglandin A1 (Table SI-1.1). The opposite migration behavior was observed for the same isomers in ESI (−), where $[M-H]^-$ or $[M-H+CH_3COONa]^-$ ions of PGA1 migrated faster than dihydroxy and hydroperoxyl isomers for the gas-phase structure of prostaglandin (Figure SI-

2.6B). Interestingly, PGA1 as $[M+Na]^+$ showed the presence of two peaks most probably due to different cationization sites (Figures SI-2.6B and 2.6C).

Overall, similar to aliphatic acyclic eicosanoids, metal adducts of prostaglandins showed better IM separation relative to the ESI (−) species. The $[M+Li]^+$ adducts of isomeric prostaglandins D2 and E2 (FA 20:4;O3) showed a ΔCCS% of 2%, and near baseline separation could be observed at $R_p \approx 120$ using HRDm (Figure 4A). Moreover, with the ΔCCS% higher than 3.5%, good separation even without HRDm could be observed for PGJ2 and PGA2 as $[M+Li]^+$ and $[M+Na]^+$ adducts (Figures 4B and 4C).

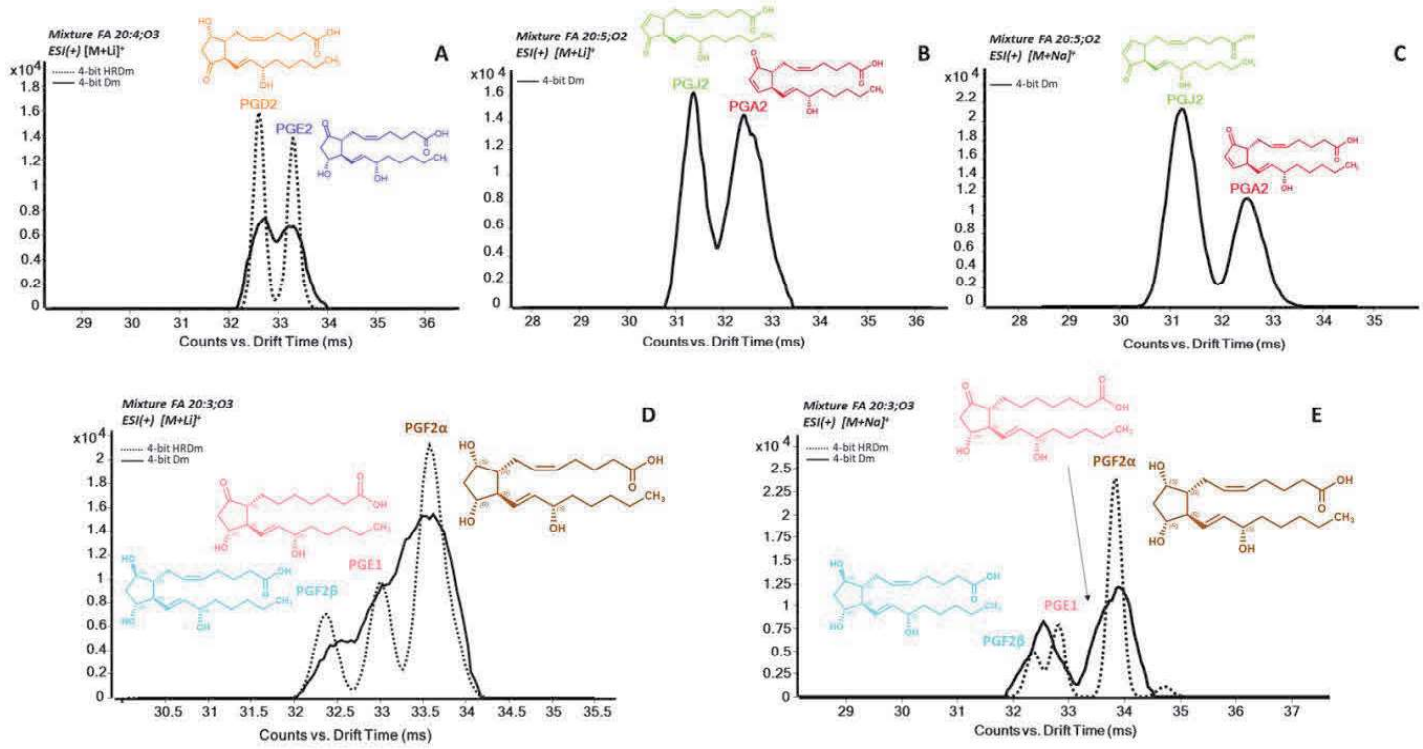

Figure 4. **Arrival time distribution for $[M+Li]^+$ adducts of FA 20:4;O3 (A) and $[M+Li]^+$ and $[M+Na]^+$ adducts of FA 20:5;O2 isomers (B and C) and FA 20:3;O3 (D and E).** PGE2: 9-oxo-11R,15S-dihydroxy-5Z,13E-prostadienoic acid. PGD2: 9S,15S-dihydroxy-11-oxo-5Z,13E-prostadienoic acid. PGJ2: 11-oxo-15S-hydroxy-5Z,9,13E-prostatrienoic acid. PGA2: 9-oxo-15S-hydroxy-5Z,10Z,13E-prostatrienoic acid. PGE1: 9-oxo-11R,15S-dihydroxy-13E-prostaenoic acid. PGF2α: 9S,11R,15S-trihydroxy-5Z,13E-prostadienoic acid. PGF2β: 9R,11R,15S-trihydroxy-5Z,13E-prostadienoic acid. Dm: 4-bit demultiplexing. HRDm: high resolution demultiplexing.

Separation of FA 20:3;O3 isomers provided an intriguing example of how adduct chemistry can change IM behavior. While PGF2α has a large structure in the gas phase, its enantiomer PGF2β assumes a compact form. Although PGE1, the third component of the FA 20:3;O3 mixture, has a structure that is noticeably distinct from other PGF isomers, it migrated in the IM space between PGF2α or PF2Fβ, both as Na and Li adducts (Figure 4D-E). The *cis*-type hydroxy groups form a more open structure, meanwhile, the *trans*-OH generates compact structures and the oxo (planar) migrates between the two former stereoisomers.

3.3. Investigating the potential of IM to improve peak capacity in the analysis of oxidized complex lipids

In order to evaluate the separation capabilities of IM for complex oxidized lipids, one polar (PC 16:0/18:2) and two neutral lipids (TG 16:0/16:0/18:2 and CE 18:2) were oxidized *in vitro* and analyzed by RPLC-DTIM-MS in ESI(+) mode for the neutral lipids and both, ESI(+) and ESI(−), for the polar lipid.

The resolving power of low-pressure DTIM instruments depends upon the length of the drift cell, electric field, charge, and buffer gas temperature.[19] Therefore, in preliminary experiments, the unoxidized lipid standards were first injected at low (12 V/cm) and high (17 V/cm) fields to investigate the effect of the electric field on the diffusion-limited resolving power.[49] An average increase of 7% of R_p was observed with the higher electric field. As originally expected, the increase of the electric field improved resolving power by reducing peak broadening.[50] Interestingly, a longer temporal separation in the low electric field allowed for improved resolution using HRDm for oxidized TG (Figure SI-2.7). Therefore, the evaluation of the optimal drift entrance and exit voltages for the optimal electric field for isomeric separation was an important parameter for data acquisition.

Liquid chromatography was coupled to the IM-MS method using a previously optimized methodology which contained ammonium formate as a mobile phase modifier (Table SI-2.1).[8] When formate or acetate salts are added, PC lipids ionize as $[M+HCOO]^-$ or $[M+CH_3COO]^-$, respectively, resulting in an informative MS/MS spectrum for both unmodified and oxidized PC.[51] For oxidized TG and CE, information about the type and position of modifications can be obtained with alkali adducts such as $[M+Na]^+$, while the addition of ammonium-containing salts in the mobile phase can affect ionization efficiency due to ion competition during ESI.[44] In IM-All Ions mode, DIA alternating between low and high collision energy frames was used. As fragmentation occurs after DTIM separation, fragments are aligned with the precursor by their drift time. However, fragments of adducts with similar mobility behavior can overlap using AIF. Ammonium salts were therefore removed from the mobile phase in ESI(+) after initial evaluations. As a result, $[M+NH_4]^+$ adducts were not detected for CE 18:2. For TG 16:0/16:0/18:2, the intensity of the $[M+Na]^+$ was increased by a factor of two. The MS/MS spectra for the sodiated adducts without ammonium salts in the mobile phase are shown in Figures SI-2.8 and SI-2.9.

Because individual standards for complex oxidized lipids are not available, *in vitro* oxidation is an appropriate strategy for future method optimization. When complex lipids are oxidized *in vitro*, a large number of species are formed, including truncated and full-length oxygenated species. Complex lipids with an increasing number of double bonds have more possibilities of oxygen addition at various positions. Therefore, separation by liquid chromatography alone might not be sufficient to resolve certain isomers. For example, CE 18:2<+1O,-2H> is an oxidized metabolite that elutes 2 min before the unmodified CE 18:2 (Figure 5). By selecting a RT window of 0.3 min (22.0-22.3), the low IM resolution data used to acquire

MS/MS data shows that a mixture of different isomers can be detected in different mobility regions (Figure 5C-D) indicating the formation of CE 18:2<oxo> isomers at different positions (9, 10, 11). The potential isomers of CE 18:2<+1O,-2H> were well discriminated by the HRDm. However, since no MS/MS data could be obtained while using 4-bit multiplexing, there was no reliable way to determine which peak corresponds to which isomer to calculate CCS values. In agreement with cationized oxylipins, epoxy modifications of CE 18:2 produce more compact structures than keto and hydroxy derivatives. Consequently, the signal migrating after CE 18:2<oxo{9}> (Figure 5B) is likely to have a keto modification that is closer to the cholesteryl moiety. The CE 18:2<+1O> modified lipid, on the other hand, has one DBE less and elutes later in the chromatogram, yielding fewer isomeric possibilities, as also shown by the HRDm data (Figure SI-2.11), and the detected species could be annotated as CE 18:1<ep> isomers.

The addition of two oxygens to esterified linoleate can result in an even more complex mixture of isomers, including a hydroperoxy group at carbons 9 and 13, or combinations of di-hydroxy, keto, or epoxy derivatives.[8] The extracted ion chromatogram of CE 18:2<+2O> is highly populated and AIF data from IM frames extracted between 21.9 and 22.2 minutes show that different isomeric CE 18:2<+2O> species are present with position-specific fragments of hydroperoxy at least at positions 9, 11, and 13 (Figure SI-2.12). The HRDm indicates that more isomeric lipids could be found in this region with an R_p of about 160, but additional MS/MS spectra are required for confirmation. According to these preliminary findings, oxidized CEs are excellent candidates for IM separation using instruments that have a resolving power higher than 150.

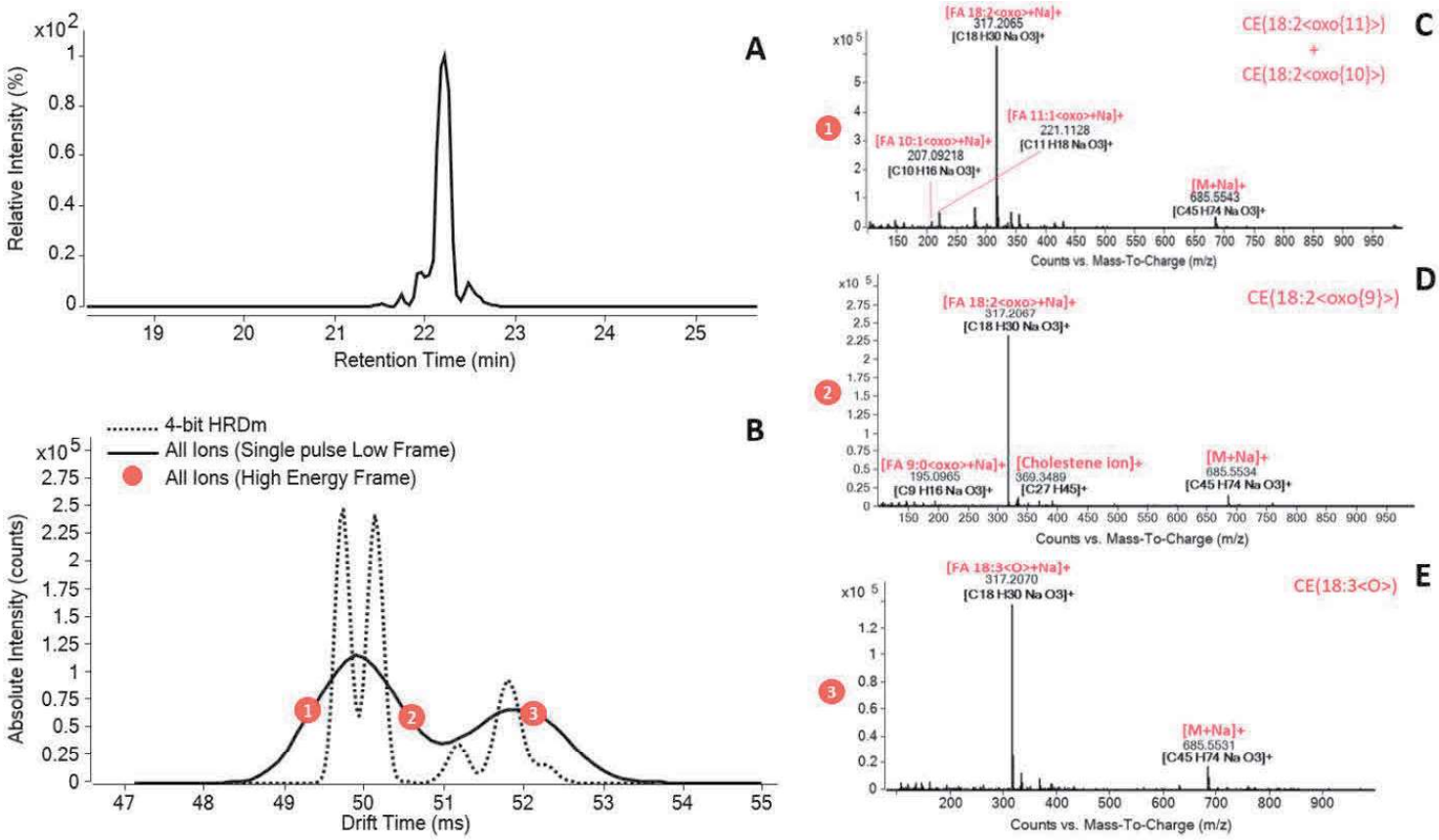

Figure 5. Reversed-phase elution of $[C_{45}H_{74}O_3+Na]^+$ assigned as CE(18:2<+1O,-2H>) (A). Arrival time distribution of high resolution demultiplexed (HRDm) ion mobility data (without MS/MS) and All ions ion mobility separation (low resolution mode with data independent acquisition) (B). MS/MS spectrum at collision induced dissociation of 40 eV for sodium adducts within 49-53 ms (C-E). FA: fatty acid.

In comparison to CE, TG lipids have more labile structures in the gas phase, as evidenced by the wider IM peaks for their sodium adducts at the same electric field. The separation of oxidized TG isomers, such as the isomers of TG 16:0/16:0/18:2<+1O,-2H> and TG 16:0/16:0/18:2<+2O,-2H> was visible at $R_s \geq 190$ (Figures SI-2.13 and SI-2.14). Although the IM separation was detected at lower dilution levels (1:10 and 1:100), proving that observed separation is not a data artifact, AIF spectra did not show position-specific fragments in the low MS range, which otherwise could have been used to confirm the presence of additional positional isomers.

The analysis of oxidized glycerophospholipids in ESI(−) allowed to obtain information about the fatty acyl composition.[8] The oxidized species PC 16:0/18:2<2O> generated various isomers located in different regions of the chromatogram due to different polarities induced by the modification types (Figure SI-2.15). The power of LC-IM for oxidized PC isomers can be illustrated using HRDm with a resolving power higher than 200, which enables different IM peak profiles at different RT regions (Figure SI-2.15A). Whereas just one IM peak is shown at an RT ≈ 15.3 min, duplets are seen at a lower RT of about 15.0 min and 14.8 min, indicating the presence of isomeric species. In the AIF spectra, intense water loss from the precursor after demethylation $[M\text{-}CH_3\text{-}H_2O]^-$ and the methylation of FA 18:3<O> moiety was seen (Figure SI-2.15C). This latter suggests that the three partially resolved chromatographic peaks (RT: 14.5-15.5 min) might represent two positional isomers of hydroperoxyl species as well as an FA 18:1<OH, oxo> isomer. As the fragment ions at the lower range are close to the noise level, it was not possible to determine the position of the modification even when applying higher collision energy. However, by increasing the number of poorly resolved peaks in LC from 3 to 5 IM peaks (Figure SI-2.15B), the peak capacity was improved by introducing IMS into the analytical workflow. For in-depth characterization, the sensitivity and mass accuracy in the high energy frame can be problematic, particularly as oxidized lipids are detected at low levels in biological samples which would require a targeted IM-MS approach. Nevertheless, this study demonstrated that DTIM-AIF can offer sufficient information to distinguish between modified and unmodified lipids that might coelute in LC.

4. Conclusions

The generation of CCS libraries using various ionization species is a useful tool to assess which ions provide the best isomeric separation. Post-processing techniques, such as HRDm, can generate data artifacts and optimization of data processing as well as analysis of dilution series for the samples in question are crucial to identify and confirm isomeric separations. The increased peak capacity that arises when combining LC and IM suggests that epilipidomics studies have enormous potential, but they require highly sensitive and

fast IM-MS instruments capable of resolving isomers as well as producing high-quality MS/MS spectra for the identification of position- and modification-specific fragments ions. Furthermore, peak capacity in MS-based lipidomics is impacted by false annotation of features due to overlapping isotopic peaks originating from different molecular species (i.e., type II isotopic effects), especially when addressing isomeric species.[52] Isotopic type II correction is generally more critical in shotgun lipidomics because no prior chromatographic separation is performed.[53] However, due to the large number of isomers with only slightly different polarity, overlaps of isotopologues with another co-eluting oxidized species can occur more often in epilipidomics analysis than in traditional LC-based lipidomics. By using IM, the isotopic type II effect can be reduced, and the intensity of a signal characterized by an *m/z* value at a specific retention time and drift time can be compared separately from the isotopologues of another co-eluting peak (Figure SI-2.16). Overall, this study shows the value of IMS in LC-HRMS workflows for the separation of highly isomeric mixtures of epilipids, but it also emphasizes the need for further development and optimization of IMS methods for epilipid analysis, as well as the importance of careful evaluation prior to assigning isomeric ions in the gas phase.

Supporting Information

Supporting Information 1.

Table SI1.1. Database of oxylipins including different ionization species, *m/z*, experimental drift tube collision cross section (CCS) values and precision measurements (standard deviation (SD), relative standard deviation (RSD)). Different isomeric groups are highlighted by different colours. ND: Non-Detected.

Table SI-1.2. Percentage difference in collision cross section (ΔCCS%) for the isomeric pairs of oxylipins.

Table SI-1.3. Literature curated collision cross section (CCS) in Å² values of oxylipins.

Supporting Information 2.

Table SI-2.1. Detailed LC and MS parameters used in the study.

Figure SI-2.1. Tandem mass spectra of FA 20:4;O isomers [M-H]- and [M-H+CH3COONa]-. 5-HETE: 5-hydroxyeicosatetraenoic acid. 15-HETE: 15-hydroxy-5Z,8Z,11Z,13E-eicosatetraenoic acid. 14,15-EpETrE: 14,15-epoxy-5Z,8Z,11Z-eicosatrienoic acid.

Figure SI-2.2A. Tandem mass spectra of FA 20:5;O isomers $[M-H]^-$ and $[M-H+CH_3COONa]^-$. 5-OxoETE: 5-oxo-6E,8Z,11Z,14Z-eicosatetraenoic acid. 15-OxoETE: 15-oxo-5Z,8Z,11Z,13E-eicosatetraenoic acid.

Figure SI-2.2B. Tandem mass spectra of FA 20:5;O isomers $[M-H]^-$ and $[M-H+CH_3COONa]^-$. 14(15)-EpETE: (+/-)-14(15)-epoxy-5Z,8Z,11Z,17Z-eicosatetraenoic acid. 15(S)-HEPE: 15S-hydroxy-5Z,8Z,11Z,13E,17Z-eicosapentaenoic acid.

Figure SI-2.3A. Tandem mass spectra of $[M+Li]^+$ adducts of (+/-)-14(15)-epoxy-5Z,8Z,11Z,17Z-eicosatetraenoic acid (14(15)-EpETE) and 15-hydroxy-5Z,8Z,11Z,13E,17Z-eicosapentaenoic acid (15-HEPE).

Figure SI-2.3B. Tandem mass spectra of $[M-H+Ba]^+$ adducts of (+/-)-14(15)-epoxy-5Z,8Z,11Z,17Z-eicosatetraenoic acid (14(15)-EpETE) and 15-hydroxy-5Z,8Z,11Z,13E,17Z-eicosapentaenoic acid (15-HEPE).

Figure SI-2.4A. Tandem mass spectra of $[M+Li]^+$ adducts of 15-oxo-5Z,8Z,11Z,13E-eicosatetraenoic acid (15-OxoETE) and 5-oxo-6E,8Z,11Z,14Z-eicosatetraenoic acid (5-Oxo-ETE).

Figure SI-2.4B. Tandem mass spectra of $[M-H+Ba]^+$ adducts of 15-oxo-5Z,8Z,11Z,13E-eicosatetraenoic acid (15-OxoETE) and 5-oxo-6E,8Z,11Z,14Z-eicosatetraenoic acid (5-Oxo-ETE).

Figure SI-2.5. Tandem mass spectra of $[M+Li]^+$ of 9S,15S-dihydroxy-11-oxo-5Z,13E-prostadienoic acid (PGD2) and 9-oxo-11R,15S-dihydroxy-5Z,13E-prostadienoic acid (PGE2).

Figure SI-2.6. Arrival time distribution for the $[M+Ag]^+$ adducts of a mixture of isomeric oxidized fatty acid (FA 20:4;O) (A), the $[M-H+CH_3COONa]^-$ and $[M+Na]^+$ adducts of FA 20:4;O2 (B and C, respectively) using 4-bit demultiplexing (Dm) and processing with high resolution demultiplexing (HRDm). The peaks were assigned based on the $^{DT}CCS_{N2}$ values. PGA1: 9-oxo-15S-hydroxy-10Z,13E-prostadienoic acid. 5(S),12(S)-DiHETE: 5S,12S-dihydroxy-6E,8Z,10E,14Z-eicosatetraenoic acid. 8(S),15(S)-DiHETE: 8S,15S-dihydroxy-5Z,9E,11Z,13E-eicosatetraenoic acid. 5(S)-HETE: 5S-hydroxyeicosatetraenoic acid. 15(R)-HETE: 15R-hydroxy-5Z,8Z,11Z,13E-eicosatetraenoic acid. 15(S)-HETE: 15S-hydroxy-5Z,8Z,11Z,13E-eicosatetraenoic acid. 14,15-EpETrE: 14,15-epoxy-5Z,8Z,11Z-eicosatrienoic acid.

Figure SI-2.7. High resolution demultiplexing separation of a sodium adduct ion of a triacylglycerol with addition of one oxygen TG(50:2<O>) using electric field of 17 *vs* 12 V/cm. TG: Triacylglycerol.

Figure SI-2.8. Reversed phased liquid chromatographic elution (A) and MS/MS spectrum at collision induced dissociation of 40 eV (B) of the unmodified CE 18:2. FA: Fatty acid. CE: Cholesterol ester.

Figure SI-2.9. Reversed phased liquid chromatographic elution (A) and MS/MS spectra at collision induced dissociation of 40 eV for $[M+Na]^+$ (B) and $[M+NH_4]^+$ (C) of the unmodified TG 16:0/16:0/18:2. FA: Fatty acid. TG: Triacylglycerol.

Figure SI-2.10A. Reversed phased liquid chromatographic elution (A) and MS/MS spectra at collision induced dissociation of 20 eV for $[M+Na]^+$ (B) and $[M+H]^+$ (C) of the unmodified PC 16:0/18:2. PC: Phosphocholine.

Figure SI-2.10B. Reversed phased liquid chromatographic elution (A) and MS/MS spectra at collision induced dissociation of 20 eV for $[M+CH_3COO]^-$ (B) and $[M+HCOO]^-$ (C) of the unmodified PC 16:0/18:2. FA: Fatty acid. PC: Phosphocholine.

Figure SI-2.11. Reversed-phase elution of $[C_{45}H_{76}O_3+Na]^+$ assigned as CE(18:1<ep>) (A). Arrival time distribution of high resolution demultiplexed (HRDm) ion mobility data (without MS/MS) and All ions ion mobility separation (low resolution mode with data independent acquisition) (B). MS/MS spectrum at collision induced dissociation of 40 eV for sodium adduct within 49-51 ms (C). FA: Fatty acid. CE: Cholesterol ester.

Figure SI-2.12. Reversed-phase elution of $[C_{45}H_{76}O_4+Na]^+$ assigned as CE(18:2<+2O>) (A). Arrival time distribution of high resolution demultiplexed (HRDm) ion mobility data (without MS/MS) and All ions ion mobility separation (low resolution mode with data independent acquisition) (B). MS/MS spectra at collision induced dissociation of 40 eV for sodium adduct within 49-51 ms (C) and 51-53 ms (D). FA: Fatty acid. CE: Cholesterol ester.

Figure SI-2.13. Reversed-phase elution of $[C_{53}H_{96}O_7+Na]^+$ assigned as TG (16:0/16:0/18:2<+1O,-2H>) (A). Arrival time distribution of high resolution demultiplexed (HRDm) ion mobility data (without MS/MS) and All ions ion mobility separation (low resolution mode with data independent acquisition) (B). MS/MS spectrum at collision induced dissociation of 40 eV for sodium adduct within 53-56 ms (C). FA: Fatty acid. TG: Triacylglycerol.

Figure SI-2.14. Reversed-phase elution of $[C_{53}H_{96}O_8+Na]^+$ assigned as TG (16:0/16:0/18:2<+2O,-2H>) (A). Arrival time distribution of high resolution demultiplexed (HRDm) ion mobility data (without MS/MS) and All ions ion mobility separation (low resolution mode with data independent acquisition) (B). MS/MS spectrum at collision induced dissociation of 40 eV for sodium adduct within 53.5-56 ms (C). FA: Fatty acid. TG: Triacylglycerol.

Figure SI-2.15. Reversed-phase elution of $[C_{42}H_{80}O_{10}NP+CH_3COO]^-$ assigned as PC(16:0/18:2<2O>) (A). Arrival time distribution of high resolution demultiplexed (HRDm) ion mobility data (without MS/MS) and All ions ion mobility separation (low resolution mode with data independent acquisition) (B). MS/MS spectra at collision induced dissociation of 20 eV for acetate adducts within 49-52 ms (C). FA: Fatty acid. PC: Glycerophosphatidylcholine.

Figure SI-2.16. Extracted ion chromatogram of the *m/z* 848.5658 showing multiple isomers (A). High resolution ion mobility demultiplexed data showing the separation between the third isotope of the *m/z* 846.5502 and *m/z* 848.5658 (B). The All ions fragmentation spectra at collision induced dissociation of 40 eV for PC(16:0/18:2<2O>) (C) and PC(16:0/18:2<OH, oxo>) (D) found in the retention time of ~13.7 min. FA: Fatty acid. PC: Glycerophosphatidylcholine.

Acknowledgements

This publication is based upon work performed in the frame of the COST Action EpiLipidNET, Pan-European Network in Lipidomics and Epilipidomics (CA19105; https://www.epilipid.net), supported by COST (European Cooperation in Science and Technology). KMdS was funded by the University of Antwerp (BOF DOCPRO 4-Antigoon ID 36893). MF lab is supported by ‘‘Sonderzuweisung zur Unterstützung profilbestimmender Struktureinheiten 2021’’ by the SMWK, TG70 by Sächsische Aufbaubank and SMWK, the measure is co-financed with tax funds on the basis of the budget passed by the Saxon state parliament (to M.F.), Deutsche Forschungsgemeinschaft (FE 1236/5-1 to M.F.), and Bundesministerium für Bildung und Forschung (01EJ2205A, FERROPath to M.F.). EI is funded by FWO-project number 1161620N.

References

(1) Ni, Z.; Goracci, L.; Cruciani, G.; Fedorova, M. Computational Solutions in Redox Lipidomics – Current Strategies and Future Perspectives. *Free Radic. Biol. Med.* **2019**, *144* (February), 110–123. https://doi.org/10.1016/j.freeradbiomed.2019.04.027.

(2) Gladine, C.; Ostermann, A. I.; Newman, J. W.; Schebb, N. H. MS-Based Targeted Metabolomics of Eicosanoids and Other Oxylipins: Analytical and Inter-Individual Variabilities. *Free Radic. Biol. Med.* **2019**, *144*, 72–89. https://doi.org/https://doi.org/10.1016/j.freeradbiomed.2019.05.012.

(3) Astarita, G.; Kendall, A. C.; Dennis, E. A.; Nicolaou, A. Targeted Lipidomic Strategies for Oxygenated Metabolites of Polyunsaturated Fatty Acids. *Biochim. Biophys. Acta - Mol. Cell Biol. Lipids* **2015**, *1851* (4), 456–468. https://doi.org/10.1016/j.bbalip.2014.11.012.

(4) Hinz, C.; Liggi, S.; Mocciaro, G.; Jung, S.; Induruwa, I.; Pereira, M.; Bryant, C. E.; Meckelmann, S. W.; O'Donnell, V. B.; Farndale, R. W.; Fjeldsted, J.; Griffin, J. L.; O'Donnell, V. B.; Farndale, R. W.; Fjeldsted, J.; Griffin, J. L. A Comprehensive UHPLC Ion Mobility Quadrupole Time-of-Flight Method for Profiling and Quantification of Eicosanoids, Other Oxylipins, and Fatty Acids. *Anal. Chem.* **2019**, *91* (13), 8025–8035. https://doi.org/10.1021/acs.analchem.8b04615.

(5) Liebisch, G.; Fahy, E.; Aoki, J.; Dennis, E. A.; Durand, T.; Ejsing, C. S.; Fedorova, M.; Feussner, I.; Griffiths, W. J.; Köfeler, H.; Merrill, A. H.; Murphy, R. C.; O'Donnell, V. B.; Oskolkova, O.; Subramaniam, S.; Wakelam, M. J. O.; Spener, F.; O, V. B.; Oskolkova, O.; Subramaniam, S.; O Wakelam, M. J.; Spener, F. Update on LIPID MAPS Classification, Nomenclature, and Shorthand Notation for MS-Derived Lipid Structures. *J. Lipid Res.* **2020**, *61* (12), 1539–1555. https://doi.org/10.1194/jlr.S120001025.

(6) Vvedenskaya, O.; Rose, T. D.; Knittelfelder, O.; Palladini, A.; Wodke, J. A. H.; Schuhmann, K.; Ackerman, J. M.; Wang, Y.; Has, C.; Brosch, M.; Thangapandi, V. R.; Buch, S.; Züllig, T.; Hartler, J.; Köfeler, H. C.; Röcken, C.; Coskun, Ü.; Klipp, E.; Von Schoenfels, W.; Gross, J.; Schafmayer, C.; Hampe, J.; Pauling, J. K.; Shevchenko, A. Nonalcoholic Fatty Liver Disease Stratification by Liver Lipidomics. *J. Lipid Res.* **2021**, *62*. https://doi.org/10.1016/J.JLR.2021.100104.

(7) Melo, T.; Domingues, P.; Ferreira, R.; Milic, I.; Fedorova, M.; Santos, S. M.; Segundo, M. A.; Domingues, M. R. M. Recent Advances on Mass Spectrometry Analysis of Nitrated Phospholipids. *Anal. Chem.* **2016**, *88* (5), 2622–2629. https://doi.org/10.1021/acs.analchem.5b03407.

(8) Criscuolo, A.; Nepachalovich, P.; Fernando, D.; Rio, G.-D.; Lange, M.; Ni, Z.; Baroni, M.; Cruciani, G.; Goracci, L.; Blüher, M.; Fedorova, M.; Garcia-del Rio, D. F.; Lange, M.; Ni, Z.; Baroni, M.; Cruciani, G.; Goracci, L.; Blüher, M.; Fedorova, M. Analytical and Computational Workflow for In-Depth Analysis of Oxidized Complex Lipids in Blood Plasma. *Nat. Commun.*

2022, *13* (1), 6547. https://doi.org/10.1038/s41467-022-33225-9.
(9) Snyder, L. R.; Kirkland, J. J.; Dolan, J. W. *Introduction to Modern Liquid Chromatography*, Third.; Lloyd R. Snyder, Joseph J. Kirkland, J. W. D., Ed.; John Wiley & Sons, Inc.: Hoboken, NJ, USA, 2009. https://doi.org/10.1002/9780470508183.
(10) Kortz, L.; Dorow, J.; Becker, S.; Thiery, J.; Ceglarek, U. Fast Liquid Chromatography–Quadrupole Linear Ion Trap-Mass Spectrometry Analysis of Polyunsaturated Fatty Acids and Eicosanoids in Human Plasma. *J. Chromatogr. B* **2013**, *927*, 209–213. https://doi.org/10.1016/j.jchromb.2013.03.012.
(11) Ianni, F.; Saluti, G.; Galarini, R.; Fiorito, S.; Sardella, R.; Natalini, B. Enantioselective High-Performance Liquid Chromatography Analysis of Oxygenated Polyunsaturated Fatty Acids. *Free Radic. Biol. Med.* **2019**, *144*, 35–54. https://doi.org/10.1016/j.freeradbiomed.2019.04.038.
(12) Cebo, M.; Fu, X.; Gawaz, M.; Chatterjee, M.; Lämmerhofer, M. Enantioselective Ultra-High Performance Liquid Chromatography-Tandem Mass Spectrometry Method Based on Sub-2µm Particle Polysaccharide Column for Chiral Separation of Oxylipins and Its Application for the Analysis of Autoxidized Fatty Acids and Platelet R. *J. Chromatogr. A* **2020**, *1624*. https://doi.org/10.1016/J.CHROMA.2020.461206.
(13) Quaranta, A.; Zöhrer, B.; Revol-Cavalier, J.; Benkestock, K.; Balas, L.; Oger, C.; Keyes, G. S.; Wheelock, Å. M.; Durand, T.; Galano, J.-M.; Ramsden, C. E.; Hamberg, M.; Wheelock, C. E. Development of a Chiral Supercritical Fluid Chromatography–Tandem Mass Spectrometry and Reversed-Phase Liquid Chromatography–Tandem Mass Spectrometry Platform for the Quantitative Metabolic Profiling of Octadecanoid Oxylipins. *Anal. Chem.* **2022**, *94* (42), 14618–14626. https://doi.org/https://doi.org/10.1021/acs.analchem.2c02601.
(14) Xu, M.; Legradi, J.; Leonards, P. Evaluation of LC-MS and LC×LC-MS in Analysis of Zebrafish Embryo Samples for Comprehensive Lipid Profiling. *Anal. Bioanal. Chem.* **2020**, *412* (18), 4313–4325. https://doi.org/10.1007/s00216-020-02661-1.
(15) Olfert, M.; Bäurer, S.; Wolter, M.; Buckenmaier, S.; Brito-de la Fuente, E.; Lämmerhofer, M. Comprehensive Profiling of Conjugated Fatty Acid Isomers and Their Lipid Oxidation Products by Two-Dimensional Chiral RP×RP Liquid Chromatography Hyphenated to UV- and SWATH-MS-Detection. *Anal. Chim. Acta* **2022**, *1202*, 339667. https://doi.org/10.1016/j.aca.2022.339667.
(16) Kyle, J. E.; Zhang, X.; Weitz, K. K.; Monroe, M. E.; Ibrahim, Y. M.; Moore, R. J.; Cha, J.; Sun, X.; Lovelace, E. S.; Wagoner, J.; Polyak, S. J.; Metz, T. O.; Dey, S. K.; Smith, R. D.; Burnum-Johnson, K. E.; Baker, E. S. Uncovering Biologically Significant Lipid Isomers with Liquid Chromatography, Ion Mobility Spectrometry and Mass Spectrometry. *Analyst* **2016**, *141* (5), 1649–1659. https://doi.org/10.1039/c5an02062j.
(17) da Silva, K. M.; Iturrospe, E.; Heyrman, J.; Koelmel, J. P.; Cuykx, M.; Vanhaecke, T.; Covaci, A.; van Nuijs, A. L. N. Optimization of a Liquid Chromatography-Ion Mobility-High Resolution Mass Spectrometry Platform for Untargeted Lipidomics and Application to HepaRG Cell Extracts. *Talanta* **2021**, *235*, 122808. https://doi.org/10.1016/j.talanta.2021.122808.
(18) Causon, T. J.; Hann, S. Theoretical Evaluation of Peak Capacity Improvements by Use of Liquid Chromatography Combined with Drift Tube Ion Mobility-Mass Spectrometry. *J. Chromatogr. A* **2015**, *1416*, 47–56. https://doi.org/10.1016/j.chroma.2015.09.009.
(19) Dodds, J. N.; Baker, E. S. Ion Mobility Spectrometry: Fundamental Concepts, Instrumentation, Applications, and the Road Ahead. *J. Am. Soc. Mass Spectrom.* **2019**, *30* (11), 2185–2195. https://doi.org/10.1007/s13361-019-02288-2.
(20) Blaženović, I.; Shen, T.; Mehta, S. S.; Kind, T.; Ji, J.; Piparo, M.; Cacciola, F.; Mondello, L.; Fiehn, O. Increasing Compound Identification Rates in Untargeted Lipidomics Research with Liquid Chromatography Drift Time-Ion Mobility Mass Spectrometry. *Anal. Chem.* **2018**, *90* (18), 10758–10764. https://doi.org/10.1021/acs.analchem.8b01527.
(21) Koomen, D. C.; May, J. C.; McLean, J. A. Insights and Prospects for Ion Mobility-Mass Spectrometry in Clinical Chemistry. *Expert Rev. Proteomics* **2022**, *19* (1), 17–31. https://doi.org/10.1080/14789450.2022.2026218.
(22) Giles, K.; Ujma, J.; Wildgoose, J.; Pringle, S.; Richardson, K.; Langridge, D.; Green, M. A Cyclic

Ion Mobility-Mass Spectrometry System. *Anal. Chem.* **2019**, *91* (13), 8564–8573. https://doi.org/10.1021/acs.analchem.9b01838.
(23) May, J. C.; Knochenmuss, R.; Fjeldsted, J. C.; McLean, J. A. Resolution of Isomeric Mixtures in Ion Mobility Using a Combined Demultiplexing and Peak Deconvolution Technique. *Anal. Chem.* **2020**, *92* (14), 9482–9492. https://doi.org/10.1021/acs.analchem.9b05718.
(24) Murphy, R. C.; Barkley, R. M.; Berry, K. Z.; Hankin, J.; Harrison, K.; Johnson, C.; Krank, J.; McAnoy, A.; Uhlson, C.; Zarini, S. Electrospray Ionization and Tandem Mass Spectrometry of Eicosanoids. *Anal. Biochem.* **2005**, *346* (1), 1–42. https://doi.org/10.1016/J.AB.2005.04.042.
(25) Hadavi, D.; de Lange, E.; Jordens, J.; Mengerink, Y.; Cuyckens, F.; Honing, M. Adduct Ion Formation as a Tool for the Molecular Structure Assessment of Ten Isomers in Traveling Wave and Trapped Ion Mobility Spectrometry. **2019**. https://doi.org/10.1002/rcm.8419.
(26) Chouinard, C. D.; Wilian, V.; Cruzeiro, D.; Beekman, C. R.; Roitberg, A. E.; Yost, R. A. Investigating Differences in Gas-Phase Conformations of 25-Hydroxyvitamin D3 Sodiated Epimers Using Ion Mobility-Mass Spectrometry and Theoretical Modeling. *J. Am. Soc. Mass Spectrom* **2017**, *28*, 1497–1505. https://doi.org/10.1007/s13361-017-1673-4.
(27) Bilbao, A.; Gibbons, B. C.; Stow, S. M.; Kyle, J. E.; Bloodsworth, K. J.; Payne, S. H.; Smith, R. D.; Ibrahim, Y. M.; Baker, E. S.; Fjeldsted, J. C. A Preprocessing Tool for Enhanced Ion Mobility-Mass Spectrometry-Based Omics Workflows. *J. Proteome Res.* **2022**, *21* (3), 798–807. https://doi.org/10.1021/acs.jproteome.1c00425.
(28) Butler, K. E.; Dodds, J. N.; Flick, T.; Campuzano, I. D. G.; Baker, E. S. High-Resolution Demultiplexing (HRdm) Ion Mobility Spectrometry-Mass Spectrometry for Aspartic and Isoaspartic Acid Determination and Screening. *Anal. Chem.* **2022**, *94* (16), 6191–6199. https://doi.org/10.1021/acs.analchem.1c05533.
(29) Dodds, J. N.; May, J. C.; McLean, J. A. Correlating Resolving Power, Resolution, and Collision Cross Section: Unifying Cross-Platform Assessment of Separation Efficiency in Ion Mobility Spectrometry. *Anal. Chem.* **2017**, *89* (22), 12176–12184. https://doi.org/10.1021/acs.analchem.7b02827.
(30) Hinnenkamp, V.; Klein, J.; Meckelmann, S. W.; Balsaa, P.; Schmidt, T. C.; Schmitz, O. J. Comparison of CCS Values Determined by Traveling Wave Ion Mobility Mass Spectrometry and Drift Tube Ion Mobility Mass Spectrometry. *Anal. Chem.* **2018**, *90* (20), 12042–12050. https://doi.org/10.1021/acs.analchem.8b02711.
(31) Picache, J. A.; Rose, B. S.; Balinski, A.; Leaptrot, K. L.; Sherrod, S. D.; May, J. C.; McLean, J. A. Collision Cross Section Compendium to Annotate and Predict Multi-Omic Compound Identities. *Chem. Sci.* **2019**, *10* (4), 983–993. https://doi.org/10.1039/c8sc04396e.
(32) Stow, S. M.; Causon, T. J.; Zheng, X.; Kurulugama, R. T.; Mairinger, T.; May, J. C.; Rennie, E. E.; Baker, E. S.; Smith, R. D.; McLean, J. A.; Hann, S.; Fjeldsted, J. C. An Interlaboratory Evaluation of Drift Tube Ion Mobility-Mass Spectrometry Collision Cross Section Measurements. *Anal. Chem.* **2017**, *89* (17), 9048–9055. https://doi.org/10.1021/acs.analchem.7b01729.
(33) Erie Gabelica, V.; Shvartsburg, A. A.; Afonso, C.; Barran, P.; Benesch, J. L. P. P.; Bleiholder, C.; Bowers, M. T.; Bilbao, A.; Bush, M. F.; Campbell, J. L.; Campuzano, I. D. G. G.; Causon, T.; Clowers, B. H.; Creaser, C. S.; De Pauw, E.; Far, J.; Fernandez-Lima, F.; Fjeldsted, J. C.; Giles, K.; Groessl, M.; Hogan, C. J.; Hann, S.; Kim, H. I.; Kurulugama, R. T.; May, J. C.; McLean, J. A.; Pagel, K.; Richardson, K.; Ridgeway, M. E.; Ed, F.; Rosu, E.; Sobott, F.; Thalassinos, K.; Valentine, S. J.; Wyttenbach, T.; Gabelica, V.; Shvartsburg, A. A.; Afonso, C.; Barran, P.; Benesch, J. L. P. P.; Bleiholder, C.; Bowers, M. T.; Bilbao, A.; Bush, M. F.; Campbell, J. L.; Campuzano, I. D. G. G.; Causon, T.; Clowers, B. H.; Creaser, C. S.; De Pauw, E.; Far, J.; Fernandez-Lima, F.; Fjeldsted, J. C.; Giles, K.; Groessl, M.; Hogan, C. J.; Hann, S.; Kim, H. I.; Kurulugama, R. T.; May, J. C.; McLean, J. A.; Pagel, K.; Richardson, K.; Ridgeway, M. E.; Rosu, F.; Sobott, F.; Thalassinos, K.; Valentine, S. J.; Wyttenbach, T. Recommendations for Reporting Ion Mobility Mass Spectrometry Measurements. *Mass Spectrom. Rev.* **2019**, *38* (3), 291–320. https://doi.org/10.1002/mas.21585.
(34) Cuykx, M.; Negreira, N.; Beirnaert, C.; Van den Eede, N.; Rodrigues, R.; Vanhaecke, T.; Laukens,

K.; Covaci, A. Tailored Liquid Chromatography–Mass Spectrometry Analysis Improves the Coverage of the Intracellular Metabolome of HepaRG Cells. *J. Chromatogr. A* **2017**, *1487*, 168–178. https://doi.org/10.1016/j.chroma.2017.01.050.

(35) Wölk, M.; Milkovska-Stamenova, S.; Fedorova, M.; Hoffmann, R. Variations in the Milk Lipidomes of Two Dairy Cow Herds Fed Hay-or Silage-Based Diets over a Full Year. *Food Chem.* **2022**, *390*, 133091. https://doi.org/10.1016/j.foodchem.2022.133091.

(36) Burla, B.; Arita, M.; Arita, M.; Bendt, A. K.; Cazenave-Gassiot, A.; Dennis, E. A.; Ekroos, K.; Han, X.; Ikeda, K.; Liebisch, G.; Lin, M. K.; Loh, T. P.; Meikle, P. J.; Orešič, M.; Quehenberger, O.; Shevchenko, A.; Torta, F.; Wakelam, M. J. O.; Wheelock, C. E.; Wenk, M. R. MS-Based Lipidomics of Human Blood Plasma: A Community-Initiated Position Paper to Develop Accepted Guidelines. *J. Lipid Res.* **2018**, *59* (10), 2001–2017. https://doi.org/10.1194/jlr.S087163.

(37) Camunas-Alberca, S. M.; Moran-Garrido, M.; Sáiz, J.; Gil-de-la-Fuente, A.; Barbas, C.; Gradillas, A. Integrating the Potential of Ion Mobility Spectrometry-Mass Spectrometry in the Separation and Structural Characterisation of Lipid Isomers. *Front. Mol. Biosci.* **2023**, *10*, 129. https://doi.org/10.3389/FMOLB.2023.1112521/BIBTEX.

(38) Olajide, O. E.; Donkor, B.; Hamid, A. M. Systematic Optimization of Ambient Ionization Ion Mobility Mass Spectrometry for Rapid Separation of Isomers. *J. Am. Soc. Mass Spectrom.* **2022**, *33* (1), 160–171. https://doi.org/10.1021/jasms.1c00311.

(39) Barrientos, R. C.; Zhang, Q. Fragmentation Behavior and Gas-Phase Structures of Cationized Glycosphingolipids in Ozone-Induced Dissociation Mass Spectrometry. *J. Am. Soc. Mass Spectrom.* **2019**, *30* (9), 1609–1620. https://doi.org/10.1007/s13361-019-02267-7.

(40) Zietek, B. M.; Mengerink, Y.; Jordens, J.; Somsen, G. W.; Kool, J.; Honing, M. Adduct-Ion Formation in Trapped Ion Mobility Spectrometry as a Potential Tool for Studying Molecular Structures and Conformations. *Int. J. Ion Mobil. Spectrom.* **2018**, *21* (1–2), 19–32. https://doi.org/10.1007/s12127-017-0227-66.

(41) Hadavi, D.; Borzova, M.; Porta Siegel, T.; Honing, M. Uncovering the Behaviour of Ions in the Gas-Phase to Predict the Ion Mobility Separation of Isomeric Steroid Compounds. *Anal. Chim. Acta* **2022**, *1200*. https://doi.org/10.1016/J.ACA.2022.339617.

(42) Leaptrot, K. L.; May, J. C.; Dodds, J. N.; McLean, J. A. Ion Mobility Conformational Lipid Atlas for High Confidence Lipidomics. *Nat. Commun.* **2019**, *10* (1), 985. https://doi.org/10.1038/s41467-019-08897-5.

(43) da Silva, K. M.; Iturrospe, E.; Bars, C.; Knapen, D.; Van Cruchten, S.; Covaci, A.; van Nuijs, A. L. N. Mass Spectrometry-Based Zebrafish Toxicometabolomics: A Review of Analytical and Data Quality Challenges. *Metabolites* **2021**, *11* (9), 635. https://doi.org/10.3390/metabo11090635.

(44) Murphy, R. C. *Tandem Mass Spectrometry of Lipids*; New Developments in Mass Spectrometry; Royal Society of Chemistry: Cambridge, 2014. https://doi.org/10.1039/9781782626350.

(45) Davoli, E.; Gross, M. L. Charge Remote Fragmentation of Fatty Acids Cationized with Alkaline Earth Metal Ions. *J. Am. Soc. Mass Spectrom.* **1990**, *1* (4), 320–324. https://doi.org/10.1016/1044-0305(90)85008-A.

(46) Zheng, X.; Aly, N. A.; Zhou, Y.; Dupuis, K. T.; Bilbao, A.; Paurus, V. L.; Orton, D. J.; Wilson, R.; Payne, S. H.; Smith, R. D.; Baker, E. S. A Structural Examination and Collision Cross Section Database for over 500 Metabolites and Xenobiotics Using Drift Tube Ion Mobility Spectrometry. *Chem. Sci.* **2017**, *8* (11), 7724–7736. https://doi.org/10.1039/C7SC03464D.

(47) Rainey, M. A.; Watson, C. A.; Asef, C. K.; Foster, M. R.; Baker, E. S.; Fernández, F. M. CCS Predictor 2.0: An Open-Source Jupyter Notebook Tool for Filtering Out False Positives in Metabolomics. *Anal. Chem.* **2022**. https://doi.org/10.1021/ACS.ANALCHEM.2C03491.

(48) Hammond, V. J.; O'Donnell, V. B. Esterified Eicosanoids: Generation, Characterization and Function. *Biochim. Biophys. Acta - Biomembr.* **2012**, *1818* (10), 2403–2412. https://doi.org/10.1016/j.bbamem.2011.12.013.

(49) Kirk, A. T.; Bakes, K.; Zimmermann, S. A Universal Relationship between Optimum Drift Voltage and Resolving Power. *Int. J. Ion Mobil. Spectrom.* **2017**, *20* (3–4), 105–109. https://doi.org/10.1007/s12127-017-0219-6.

(50) Revercomb, H. E.; Mason, E. A. Theory of Plasma Chromatography/Gaseous Electrophoresis. A Review. *Anal. Chem.* **1975**, *47* (7), 970–983. https://doi.org/10.1021/ac60357a043.
(51) Ni, Z.; Sousa, B. C.; Colombo, S.; Afonso, C. B.; Melo, T.; Pitt, A. R.; Spickett, C. M.; Domingues, P.; Domingues, M. R.; Fedorova, M.; Criscuolo, A. Evaluation of Air Oxidized PAPC: A Multi Laboratory Study by LC-MS/MS. *Free Radic. Biol. Med.* **2019**, *144* (June), 156–166. https://doi.org/10.1016/j.freeradbiomed.2019.06.013.
(52) Köfeler, H. C.; Eichmann, T. O.; Ahrends, R.; Bowden, J. A.; Danne-Rasche, N.; Dennis, E. A.; Fedorova, M.; Griffiths, W. J.; Han, X.; Hartler, J.; Holčapek, M.; Jirásko, R.; Koelmel, J. P.; Ejsing, C. S.; Liebisch, G.; Ni, Z.; O'Donnell, V. B.; Quehenberger, O.; Schwudke, D.; Shevchenko, A.; Wakelam, M. J. O. O.; Wenk, M. R.; Wolrab, D.; Ekroos, K. Quality Control Requirements for the Correct Annotation of Lipidomics Data. *Nat. Commun.* **2021**, *12* (1), 4771. https://doi.org/10.1038/s41467-021-24984-y.
(53) Schuhmann, K.; Almeida, R.; Baumert, M.; Herzog, R.; Bornstein, S. R.; Shevchenko, A. Shotgun Lipidomics on a LTQ Orbitrap Mass Spectrometer by Successive Switching between Acquisition Polarity Modes. *J. Mass Spectrom.* **2012**, *47* (1), 96–104. https://doi.org/10.1002/JMS.2031.